ChemPubSoc Europe

DOI: 10.1002/chem.201504757

CHEMISTRY A European Journal Full Paper

Metal–Organic Frameworks

Study of the Discrepancies between Crystallographic Porosity and Guest Access into Cadmium–Imidazolate Frameworks and Tunable Luminescence Properties by Incorporation of Lanthanides

Suvendu Sekhar Mondal,[a] Asamanjoy Bhunia,[b] Ahmed G. Attallah,[c, d] Philipp R. Matthes,[e] Alexandra Kelling,[a] Uwe Schilde,[a] Klaus Müller-Buschbaum,[e] Reinhard Krause-Rehberg,[c] Christoph Janiak,[b] and Hans-Jürgen Holdt*[a]

Abstract: An extended member of the isoreticular family of metal–imidazolate framework structures, IFP-6 (IFP = imidazolate framework Potsdam), based on cadmium metal and an in situ functionalized 2-methylimidazolate-4-amide-5-imidate linker is reported. A porous 3D framework with 1D hexagonal channels with accessible pore windows of 0.52 nm has been synthesized by using an ionic liquid (IL) linker precursor. IFP-6 shows significant gas uptake capacity only for CO_2 and CH_4 at elevated pressure, whereas it does not adsorb N_2, H_2, and CH_4 under atmospheric conditions. IFP-6 is assumed to deteriorate at the outside of the material during the activation process. This closing of the metal–organic framework (MOF) pores is proven by positron annihilation lifetime spectroscopy (PALS), which revealed inherent crystal defects. PALS results support the conservation of the inner pores of IFP-6. IFP-6 has also been successfully loaded with luminescent trivalent lanthanide ions (Ln^{III} = Tb, Eu, and Sm) in a bottom-up one-pot reaction through the in situ generation of the linker ligand and in situ incorporation of photoluminescent Ln ions into the constituting network. The results of photoluminescence investigations and powder XRD provide evidence that the Ln ions are not doped as connectivity centers into the frameworks, but are instead located within the pores of the MOFs. Under UV light irradiation, Tb@IFP-6 and Eu@IFP-6 (λ_{exc} = 365 nm) exhibit observable emission changes to a greenish and reddish color, respectively, as a result of strong Ln 4 f emissions.

Introduction

Metal–organic frameworks (MOFs) have been subject to serious attention during the past two decades due to structure-orientated applications, such as gas storage and separation, luminescence, catalysis, sensing, and drug release.[1,2] However, for many MOFs there is a discrepancy between the theoretical surface area predicted by crystallographic considerations and experimentally determined porosity.[3] Underperformance in MOFs has been ascribed to interpenetration,[4] incomplete removal of guests from pores,[5] and pore collapse.[6] Various methodologies have been employed to achieve higher porosity.[6b,7] Direct detection and analysis of these failure modes remain difficult and can yield ambiguous results. The structural purity of previously reported MOFs was most often analyzed by powder X-ray diffraction (PXRD). PXRD can yield information about crystallinity, but is less well suited for examining disorder or defects. Gas sorption techniques provide quantitative measurements of accessible internal surface area, but are subject to kinetic limitations and do not probe closed pores.[2]

However, several compounds have a discrepancy between porosity predicted by crystallography and porosity measured by gas sorption analysis.[3] A good example is Zn-HKUST-1, for which analysis of Zn-HKUST-1 by PXRD and gas sorption indicates retention of crystalline structure, but negligible nitrogen uptake at 77 K, respectively.[8] By using positron annihilation lifetime spectroscopy (PALS), a densified surface layer that prevented the entry of even small molecular species into the crystal framework was revealed.[8] To understand this incongruity, we undertook an in-depth study with PALS to investigate the

[a] Dr. S. S. Mondal, A. Kelling, Prof. U. Schilde, Prof. H.-J. Holdt
Institut für Chemie, Anorganische Chemie
Universität Potsdam, Karl-Liebknecht-Strasse 24–25
14476 Potsdam (Germany)
Fax: (+49) 331-977-5055
E-mail: holdt@uni-potsdam.de

[b] Dr. A. Bhunia, Prof. C. Janiak
Institut für Anorganische Chemie und Strukturchemie
Heinrich-Heine-Universität Düsseldorf, Universitätsstrasse 1
40225 Düsseldorf (Germany)

[c] A. G. Attallah, Prof. R. Krause-Rehberg
Institut für Physik
Martin-Luther-Universität Halle-Wittenberg
Von-Danckelmann-Platz 3, 06120 Halle (Germany)

[d] A. G. Attallah
Physics Department, Faculty of Science
Minia University, P.O. 61519 (Egypt)

[e] Dr. P. R. Matthes, Prof. K. Müller-Buschbaum
Institut für Anorganische Chemie, Universität Würzburg
Am Hubland, 97074 Würzburg (Germany)

Supporting information for this article is available on the WWW under http://dx.doi.org/10.1002/chem.201504757.

porosity of a MOF, IFP-6 (IFP = imidazolate framework Potsdam), and to explain the behavior of the inner surface properties of the MOF.[9,10]

Light-emitting MOFs represent a class of light-emitting materials that enable color tuning by deliberate setting of the emission chromaticity.[11,12] Prominent among reported luminescent MOFs are those that contain lanthanide ions due to their metal-centered 4f–4f transitions. Even the inclusion of more than one luminescent center in MOF materials has been successful and used for color tuning. Together with sensitizer effects of the ligand, various and excellent luminescence performances have been reported.[13,14] In addition, heterostructures achieved by integrating MOFs with other functional materials show great advantages compared with pure MOFs due to their synergistic effects.[13–16] In addition to positioning, for example, lanthanide cations as connectivity centers in a MOF, the ions can also be incorporated into the pore system of a lanthanide-free MOF; the incorporation of Ln hydrate complexes was successfully shown for Pb^{II}- and Cd^{II}-containing MOFs. The lanthanide ions can thereby also participate in luminescence.[17] Rosi and co-workers investigated the encapsulation of various Ln^{III} cations into bio-MOF-1 to fabricate guest-induced luminescent materials.[17c] Su and co-workers reported a fluorescence sensor by encapsulating Ln^{III} cations in an anionic porous framework.[18] Recently, we reported the white-light emission of IFP-1 by in situ codoping of the pore system with Eu^{III} and Tb^{III}.[19] Herein, we also present the synthesis of Ln-doped IFP-6, named Ln@IFP-6 (Ln^{III} = Tb, Eu, and Sm), and a study on the photoluminescence properties.

Results and Discussion

Synthesis and structure determination

Crystalline IFP-6 ([Cd(L1)]·0.5 DMF·0.75 H_2O) was formed in a mixture of ionic liquid (IL), 3-methyl-1-octylimidazolium 4,5-dicyano-2-methylimidazolate (IL1), with $Cd(OAc)_2$·2 H_2O in DMF under solvothermal conditions (Scheme 1). 4,5-Dicyano-2-methylimidazolate, the anionic part of IL1, acts as a source of the linker and transforms into the chelating imidazolate-4-amide-5-imidate linker (L1), which forms a neutral and highly crystalline framework (Figure S1 in the Supporting Information). We have developed the synthesis of a series of isostructural MOFs, named IFPs, by using an imidazolate-4-amide-5-imidate linker, which is formed in situ under solvothermal conditions.[20] Specifically, Zn-MOF (IFP-1) was synthesized from 4,5-dicyano-2-methylimidazole (**1**) as a linker precursor, under solvothermal conditions in DMF.[20a] To obtain a new Cd-based IFP from linker **1**, we carried out several types of reactions with different Cd salts, as mentioned in the synthetic strategies for preparing zeolitic imidazolate frameworks (ZIFs; Scheme S1 in the Supporting Information), but none of the reactions yielded a framework that was isostructural to IFP-1. Hence, linker **1** was modified into an IL precursor (IL1; Scheme 1),[21] wherein the linker was preionized as the imidazolate anion, whereas the countercation, 3-methyl-1-octyl imidazolium, was not involved in coordination bonding.[22,23] We anticipated that the cation of IL1, which was large with a bulky alkyl chain, would enhance the hydrophobic character in solution, prevent favorable solvent–framework interaction, and therefore, lead to the formation of a 3D framework.[22a,24]

The structure of IFP-6 was determined by single-crystal X-ray crystallography and was found to be isostructural to that of IFP-1 with the same *etb* topology.[20a] The asymmetric unit contains one Cd^{II} ion and the bridging ligand L1 (Figure 1a). The

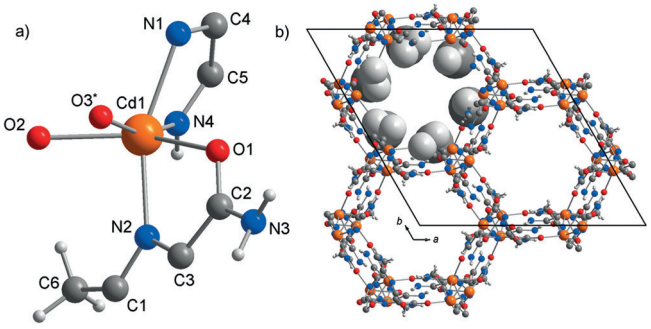

Figure 1. a) Asymmetric unit of as-synthesized IFP-6 (O3* is only 20% occupied). b) Hexagonal channels in IFP-6 (the methyl substituents at linker L1 are presented in space-filling mode (orange Cd, blue N, red O, dark gray C, light gray H)).

Cd^{II} ion is pentacoordinated by the donor atoms of three L1 ligands to form a distorted environment with a trigonal–bipyramidal geometry. In this arrangement, the two imidazolate N atoms (N1 and N2) occupy the axial positions, and the imidate N (N4) and O (O2) atoms and amide O (O1) atoms reside in the equatorial positions. Moreover, the sixth coordination mode around one-fifth of the Cd centers of the IFP-6 structure is filled by a water molecule (O3*), which shows sixfold coordination. The remaining cadmium ions are pentacoordinated. In comparison, solvent molecules are not coordinated to Zn ions in the IFP-1 structure, which forms only pentacoordination by the L1 linkers in a distorted trigonal–bipyramidal geometry (Figure S7 in the Supporting Information). The structure of IFP-6 possesses 1D hexagonal channels running along the *c* axis. The methyl groups protrude into the open channels and influence the accessible pore window (Figure 1b). By considering

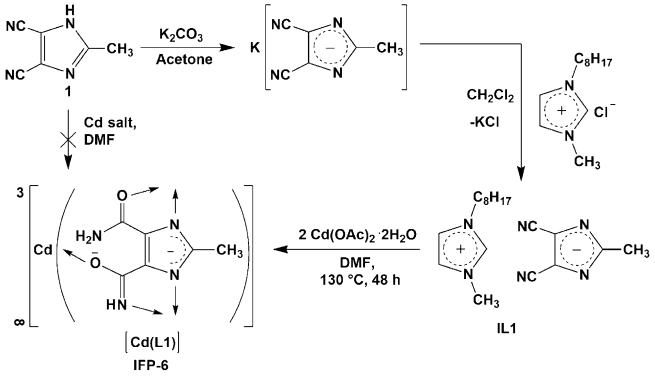

Scheme 1. Synthesis of IFP-6 from the IL precursor (IL1).

the van der Waals radii, the accessible pore window in IFP-6 was estimated to be 0.52 nm. Calculations with the PLATON toolkit indicated that IFP-6 contained 42.9% solvent-accessible space (see the Supporting Information for details). The channel diameter of IFP-6 thereby exceeds that of isostructural IFP-1 (IFP-1 (0.42 nm, $M = Zn^{II}$) < IFP-6 (0.52 nm, $M = Cd^{II}$)) as a result of the larger cation radius of Cd^{II}. Additionally, the structure is supported by IR spectroscopy (Figure S2 in the Supporting Information), PXRD patterns (Figure 2), and ^{1}H MAS and ^{13}C CP-MAS NMR spectroscopy data (Figure S5 in the Supporting Information).

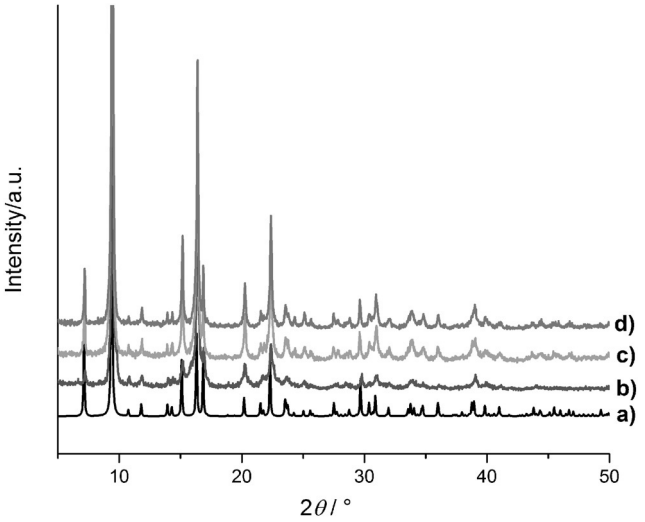

Figure 2. PXRD patterns of IFP-6: a) simulated, b) as-synthesized, c) activated, d) after gas uptake of CO_2 and CH_4.

For the synthesis of Ln@IFP-6 (Ln^{III} = Tb, Eu, and Sm) and incorporation of lanthanide ions into the IFP-6 pores, solvothermal reactions of the linker precursor IL1 and $Cd(OAc)_2 \cdot 2H_2O$ were carried out together with an equivalent of trivalent europium, terbium, or samarium nitrate. For reproducibility of the results, all reactions were repeated three times under the same conditions. Inductively coupled plasma optical emission spectroscopy (ICP OES) analysis shows that the amount of Ln ions with respect to Cd^{II} ranges from 1.3 to 1.8 at% (Table S1 in the Supporting Information). The loading of lanthanide does not affect the crystalline integrity of the material, as confirmed by PXRD results (Figure S3 in the Supporting Information). The synthesis of luminescent codoped MOFs is usually based on the statistical replacement of a certain amount of connectivity centers by luminescent ions, such as Ln^{III}, during MOF formation.[13,14] Statistical replacement thereby fundamentally depends on a match between the two different metal ions for parameters such as ionic radii, valence, and chemical reactivity. For the potential codoping of IFP-6 with lanthanide ions, these parameters do not match with those of Cd^{II}. On the other hand, the approach of in situ ligand synthesis concomitant with MOF formation is promising to immobilize highly charged ions, such as Ln^{III}, within the pore system and thereby avoid postsynthetic treatment hindered by electrostatic interactions.[17] Ideal Ln@IFP-6 contains only small amounts of Ln^{III} ions, which introduce an imbalance in the electronic equilibrium of the network. Therefore, we assume the additional intercalation of anions, such as nitrate, from the reagents and possibly formate formation, as observed for Ln@IFP-1.[19] Further charge equilibration is possible at functional groups inside the channels of the framework.

The channels of as-synthesized IFP-6 and Ln@IFP-6 contain solvent molecules. From crystallographic data of IFP-6, about 0.75 H_2O and 0.5 DMF molecules per formula unit can be estimated. The material was activated at 200 °C and 10^{-3} mbar of pressure for 48 h. PXRD patterns of the activated sample exhibited similar diffraction peaks to those of the as-synthesized framework (Figure 2). Thus, the porous framework has maintained the crystalline integrity, even without solvent molecules. Additionally, the asymmetric unit of activated IFP-6 showed fivefold coordination (Figure 3). Coordinated water and solvent

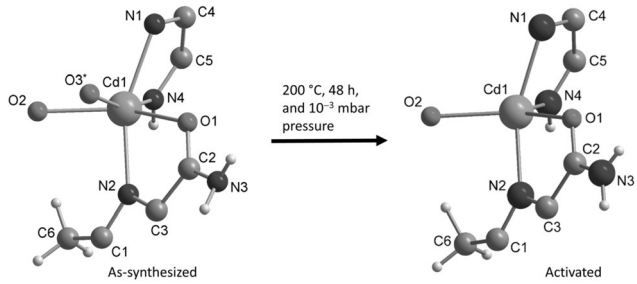

Figure 3. Asymmetric unit of activated IFP-6.

molecules in the channels were removed through the activation process with very little effect on the cell parameters and volume, showing structural identity (Figure 3 and Table S2 in the Supporting Information). The chemical stability of IFP-6 was analyzed through suspension in boiling methanol, benzene, and water for seven days; these conditions reflect extreme operational parameters of typical industrial chemical processes. After such extensive treatment, the materials maintained their fully crystalline integrity in methanol and benzene, as confirmed by PXRD (Figure S4 in the Supporting Information). In boiling water, IFP-6 irreversibly transformed into a so-far unknown crystalline phase after 24 h (Figure S4 in the Supporting Information). The reason for the instability of IFP-6 in water, in comparison to the water stability of IFP-1, is assumed to be related to the more pronounced unsaturated character of the pentacoordinated Cd^{II} center after activation.

Sorption and porosity

In principle, it was expected that IFP-6 should perform with comparable or higher gas uptake than IFP-1 because of its larger pore aperture and void volume. Surprisingly, N_2, H_2, and CH_4 cannot be adsorbed by IFP-6 at various temperatures and 1 bar, although the kinetic diameter of the gases is smaller than the effective pore window size (0.52 nm; see Figure 4a, Table 1, and Figure S11 in the Supporting Information). Finally,

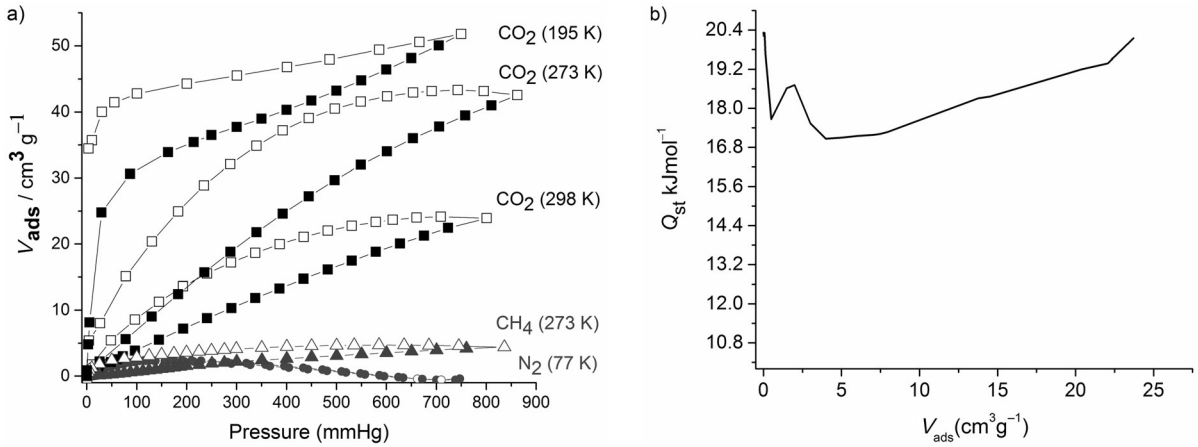

Figure 4. a) Gas sorption isotherms of IFP-6 for N_2, CO_2, and CH_4 (adsorption and desorption branches are indicated by closed and open symbols, respectively). The higher CO_2 amount upon desorption at 273 K is an artifact of the low equilibration time of 20 s per data point. At equilibration intervals of 60 and 120 s, the desorbed amount of CO_2 stays below the adsorption maximum (Table S6 and Figure S12 in the Supporting Information). Because the increasing equilibration time also increases the overall CO_2 uptake, the 273 K curve is shown herein for 20 s of equilibration for comparison with the other temperatures; b) Isosteric heats of CO_2 adsorption as a function of the adsorbent loading for IFP-6.

Table 1. Gas sorption data (in $cm^3 g^{-1}$) of IFP-6 in comparison with IFP-1.

	IFP-6	IFP-1
pore window [nm]	0.52	0.42
N_2 (77 K)	0	224.6[a]
CO_2 (298 K)	22.4	48[a]
CO_2 (273 K)	39.5 and 132.2[b]	–[c] and 156.9[b]
CO_2 (195 K)	51.7	–[c]
CH_4 (273 K)	4.2 and 87.4[b]	31.4[d] and 127.8[b]
H_2 (77 K)	1.1	168.1[a]

[a] From ref. [20a]. [b] Gas sorption data at high pressure up to 50 bar.[27] [c] Not reported. [d] Figure S11 in the Supporting Information.

we tried to activate the sample through a supercritical CO_2 activation procedure, but this also failed to exhibit a larger accessible surface area (2.7 $m^2 g^{-1}$). Compared with IFP-1, a low amount of CO_2 adsorbed by IFP-6 and a broad desorption hysteresis were observed (Figure 4a and Table 1). To understand the nature of amide–CO_2 interactions, the coverage-dependent isosteric heat of CO_2 adsorption (Q_{st}) was calculated by using a Clausius–Clapeyron equation (Figure 4b). As shown in Figure 4b, the adsorption enthalpy for CO_2 is 20.3 kJ mol^{-1} at zero coverage. Noticeably, the adsorption enthalpy value decreased at first, increased again to go through a small maximum, and finally clearly increased with increasing CO_2 uptake. Several amide-containing MOFs were reported that showed similar behavior for Q_{st} versus adsorbed CO_2 volume.[25,26] These amide-containing MOFs also exhibited a broad hysteresis and similar desorption profile, which led to the convincing interpretation of this broad desorption hysteresis as intermolecular amide interactions with CO_2 molecules based on isosteric heat measurements together with DFT calculations.[25a–c] Amide groups inside the channels can cooperatively bind CO_2 molecules (amide:CO_2). In addition, amide cooperativity permits the slipped-parallel arrangement of CO_2 molecules by amide:CO_2:CO_2:amide binding, which gives an extra gain of attraction of about -3 kJ mol^{-1}. The amide:CO_2:CO_2:amide binding interaction correlates with the significant increase in CO_2 adsorption enthalpy with increasing CO_2 uptake.[25a–c] These reported studies can explain the hysteretic CO_2 sorption behavior and heats of adsorption data of IFP-6.

To investigate the adsorption properties at higher pressures, CO_2 and CH_4 adsorption isotherms on IFP-1 and IFP-6 were reported at 273 K up to 50 bar.[27] A significant amount is adsorbed by IFP-6 at high pressure; this is comparable to IFP-1. Interestingly, IFP-6 maintained crystallinity after high-pressure gas uptake (Figure 2), whereas at least part of the IFP-6 framework broke down during the activation process to create an instability of the surface. Fractions, which turn amorphous, are not detectable by PXRD. We assume partial deterioration of the material and closing of the 1D channel pores. Therefore, the diffusion of gas molecules at atmospheric pressure is restricted, whereas at elevated pressure, gas molecules are compelled to diffuse into the pores. Such a phenomenon is not common, but has been reported for microporous MOFs.[28]

PALS

The PALS method can be applied for open- and closed-pore systems. The method can provide evidence for the presence of inner pores in solvent-free IFP-6, although the pores probably are blocked by amorphous phases. For comparison, PALS of IFP-1 was measured under similar conditions. We accumulated 5×10^7 counts for the two spectra (2.5×10^7 stored in each spectrum) of digital PALS at a counting rate of 362 s^{-1} (see the Supporting Information for details). We analyzed data with the LT10 routine and the parapositronium lifetime component (0.125 ns) was fixed along the analysis because leaving it free gave 0.240 ns and the other components were free. From Figure 5, we can see that activation corresponding to the larger pore (τ_4) became pronounced after 50 h of annealing. Also, we find that the values of positronium annihilation life-

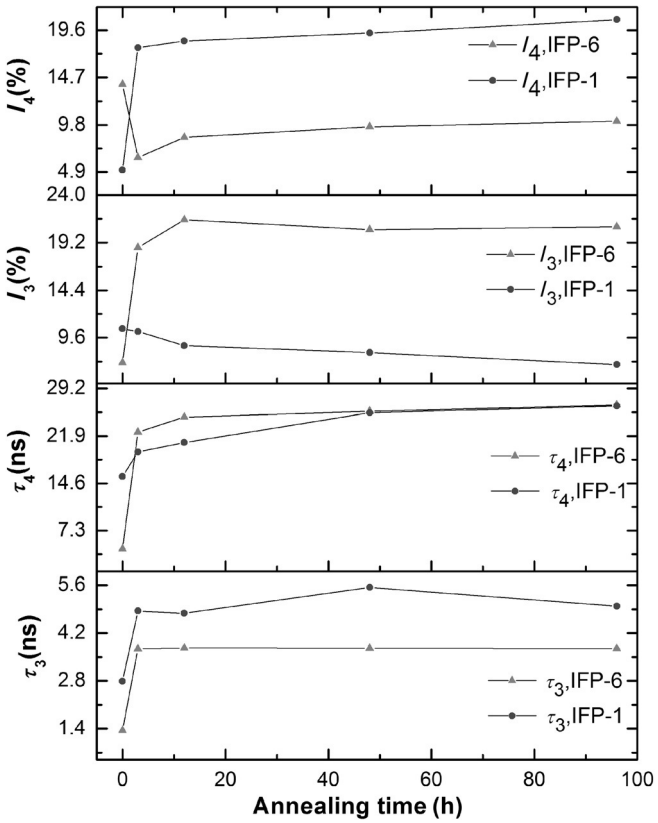

Figure 5. Lifetimes and their intensities for IFP-6 and -1 as a function of annealing time. ^{22}Na was used as a positron source.

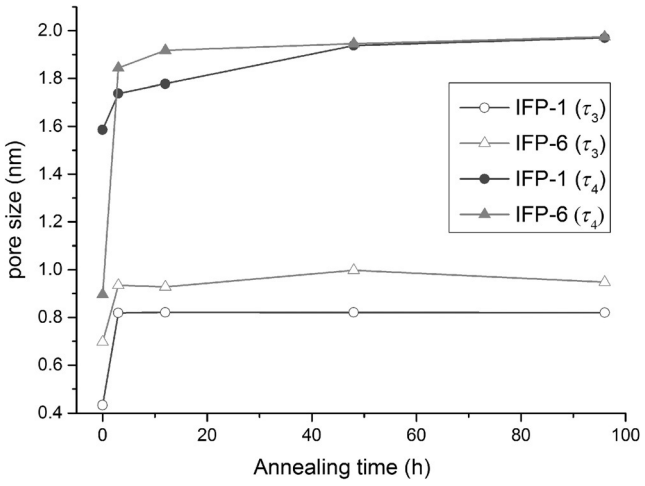

Figure 6. Pore sizes for considering the spherical shapes of IFP-6 and -1 as a function of annealing time.

time inside the material matrix or inside small pores (τ_3) is stable earlier than that inside τ_4, and the values of τ_3 for IFP-1 are slightly larger than those for IFP-6 along the activation periods. With respect to the intensities inside the pores (I_4), it can be assumed that for IFP-6 the values decrease to 12 h of activation and then become constant. This may be attributed to the annealing behavior, which causes the concentration of the pores to decrease as a result of filling of the pore windows or blocking up to 12 h and then becomes fixed. The behavior is shown for IFP-1 in Figure 5, and the intensity increased up to about 12 h and then became constant; this may be understood as an increase in the pore concentration.

The effect of activation on the pore size is shown in Figure 6 and, based on crystallographic data, we anticipate that the geometrical shape of the samples could result from spherical pores. To determine the pores size from τ_3, we assumed a constant size after solvent removal (Figure 6). From the CO_2 adsorption isotherm at 273 K, the pore size distribution was derived to be between 0.4 and 1.0 nm by using nonlocal (NL) DFT with a "CO_2 on carbon-based slit-pore model" (Figure S13 in the Supporting Information), which showed a relative maximum at about 0.98 nm; this is comparable to a small pore diameter ($\approx$0.95 nm) obtained from the pore size versus annealing time data and the value is also close to that of a small pore (1.25 nm) obtained from the X-ray structure (Figure S8 in the Supporting Information). Inside large pores ($\approx$1.95 nm), the value fits with cylindrical pores (2.04 nm) obtained from the X-ray structure of IFP-6 (Figure S8 in the Supporting Information). Moreover, the pore size behavior of IFP-6 is similar to that of IFP-1 and the τ_3 value of IFP-1 is slightly lower than that of the smaller theoretical pore size (Figure 6).

We thereby consider the behavior of IFP-6 to be reasonable due to inherent surface blocking after solvent removal, which renders it impermeable to molecular guests. The reason could be the formation of an amorphous phase, as a result of the more flexible fivefold coordination of the Cd^{II} center of activated IFP-6, which was proved by single-crystal X-ray data, than that of fivefold coordination around the Zn^{II} center in IFP-1. The crystal structure showed that 20% of Cd^{II} ions were prone to sixfold coordination, which indicated that Cd^{II} preferred higher coordination. An alternative hypothesis can be supported by the water instability of IFP-6, which attains a higher coordination number in polar water solvent. Therefore, the solvent removal process may facilitate instability at the Cd^{II} center. Hence, the amorphous material and rough surface can be generated by partial framework cleavage at the outer surface, which closes the pore window. Therefore, IFP-6 has inherent crystal defects.[29,30] At atmospheric pressure, gas molecules could probably not diffuse due to blockage by the amorphous phase, created after solvent removal, whereas, at high pressure, gases are compelled to diffuse into the pore. PALS, which is a powerful method for open- and closed-pore systems, provides complementary evidence for the porosity of the closed surface of IFP-6 and has the unique ability to uncover new phenomena in this material with nanoscale porosity.

Photoluminescence

The photoluminescence properties of IFP-6 were determined for comparison with those of Ln-doped MOFs. A weak, broad, and blue-colored emission band, ranging from $\lambda = 375$ to 700 nm, in the solid state at RT with $\lambda_{max} = 434$ nm ($\lambda_{exc} =$ 360 nm) was observed, originating from fluorescence of the linker. The MOF shows correlating featureless broad excitation bands in the range of $\lambda = 300$–425 nm, with $\lambda_{max} = 360$ nm

($\lambda_{em}=434$ nm), and is comparable to IFP-1 (Figure S15 in the Supporting Information). In addition, lifetime investigations were carried out on solid IFP-6 (see the Supporting Information); these results corroborated fluorescence through decay times of <10 ns for the process.

The photoluminescence properties of Ln@IFP-6 ($Ln^{III}=Eu$, Tb, and Sm) were also determined. The introduction of in situ available trivalent lanthanide ions into the MOF framework formation reaction leads to variable luminescence properties. The lanthanide-containing materials Ln@IFP-6 exhibit additional emission lines expected for lanthanide-centered emission due to intra 4 f–4 f transitions. For Tb@IFP-6 typical Tb^{III} transitions of $^5D_4\rightarrow{}^7F_J$ ($J=6$ at $\lambda=489$ nm, $J=5$ at $\lambda=543$ nm, $J=4$ at $\lambda=583$ nm, $J=3$ at $\lambda=620$ nm, $J=2$ at $\lambda=648$ nm, $J=1$ at $\lambda=668$ nm, $J=0$ at $\lambda=679$ nm), for Eu@IFP-6 Eu^{III} transitions of $^5D_0\rightarrow{}^7F_J$ ($J=0$ at $\lambda=579$ nm, $J=1$ at $\lambda=591$ nm, $J=2$ at $\lambda=615$ nm, $J=3$ at $\lambda=649$ nm, $J=4$ at $\lambda=698$ nm), and for Sm@IFP-6 Sm^{3+} transitions of $^4G_{5/2}\rightarrow{}^6H_J$ ($J=5/2$ at $\lambda=560$ nm, $J=7/2$ at $\lambda=596$ nm, $J=9/2$ at $\lambda=642$ nm) were observed (Figure 7). The intensities of the 4 f–4 f transitions are superimposed on the broad emission band of the nondoped framework, which retains a fluorescence maximum at $\lambda_{max}=434$ nm.

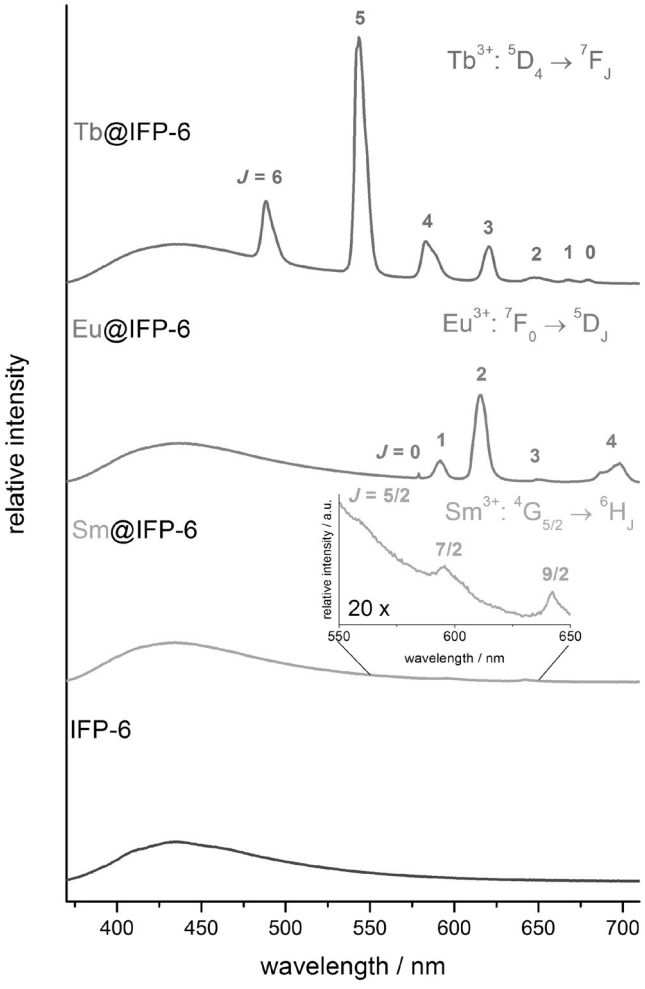

Figure 7. Normalized emission spectra of Ln@IFP-6 and IFP-6 ($\lambda_{exc}=360$ nm, from top to bottom).

As shown by the excitation spectra (see Figure S16 in the Supporting Information), there is no direct excitation of Ln^{III}. Instead, the excited Ln^{III} 4 f states are sensitized by the singlet excited states of the linker, despite their short lifetimes. Corroboration of the excitation spectra for distinct Ln^{III} emission transitions indicates such an antenna effect between the framework backbone of IFP-6 and the Ln ions; this allows activation of the Ln emission through excitation of the MOF framework.[12] Comparing the intensities of the Ln emission to the broad-band emission and to one another, Tb^{III} in Tb@IFP-6 shows the most intense emission followed by that of Eu^{III}. The intensity of the Sm^{III} metal based emission is minimal. In principle, these observations are corroborated by the incorporation of Tb^{III} and Eu^{III} into the pore system of IFP-1,[19] for which also 4 f–4 f transitions of lanthanide emission from the pore system have been reported. However, the metal-centered emission of Ln@IFP-6 proves superior to that of Ln@IFP-1 in intensity. Because no direct metal excitation is observed for either MOF, the sensitizing effect of the ligand backbone seems to be considerably stronger for IFP-6 for Cd^{II} as a connectivity center compared with Zn^{II} in IFP-1.

Furthermore, the observation of an overall broadening of the emissive 4 f–4 f transitions in all Ln^{III}-doped frameworks leads to the assumption that the Ln^{III} ions are neither located on a special site in the crystalline network nor on a single distinct crystallographic position. In comparison, crystalline Ln MOFs with Ln ions on distinct crystallographic sites within the backbone framework show much sharper line spectra, including decent rotational fine structure of the 4 f energy states for the crystalline materials.[31] The broad emission lines observed for Ln@IFP-6 assume a rather loose incorporation of the Ln^{III} ions into the cavities of the porous frameworks, which includes different plausible chemical surroundings, binding lanthanide ions to the donor groups of the MOF, and additional solvent molecules in the pores.[19] Compensation for the cationic charges inside the pore system is possible by anions, such as the original nitrates. An overlay of different coordinative surroundings lead to band broadening and a loss of line sharpness because each coordinated luminescence center contributes its own emission spectrum that differs by a few nm from the others for each transition. The feature of Ln incorporation was deliberately explored for Ln doping into IFP-1, for which similar effects were observed.[19]

The observed luminescent lifetimes for Ln@IFP-6 (τ_1, τ_2) of the linker-based fluorescent broad emission bands can be fitted with a biexponential decay on the nanosecond scale, coinciding with nondoped IFP-6 (Eu@IFP-6, 83% states subsiding at $\tau_1=1.6(1)$ ns and the remaining 17% at $\tau_2=5.9(1)$ ns; Tb@IFP-6, 86% states subsiding at $\tau_1=1.8(1)$ ns and the remaining 14% at $\tau_2=7.2(2)$ ns; Table S8 in the Supporting Information). This suggests that the incorporation of the observed 1.3–1.8 at% of Ln^{III} ions into the cavities of the framework leaves the electronic structure of the overall Cd^{II}-containing framework almost unaltered. Lifetime determinations of the parity forbidden intra-4 f–4 f Ln emissions of both Ln@IFP-6 ($Ln^{III}=Eu$ and Tb) again show biexponential decay rates on a considerably longer scale, as expected for Tb^{II} and Eu^{II}

(Eu@IFP-6, 46% of the excited states subsiding at $\tau_1 = 480(5)$ μs and 52% at $\tau_2 = 971(16)$ μs; Tb@IFP-6, 43% of the excited states subsiding at $\tau_1 = 754(10)$ μs and 55% at $\tau_2 = 1426(19)$ μs; see also Table S8 in the Supporting Information). The lifetimes of the lanthanide- and linker-based emissions differ by orders of magnitude. Therefore, the overall process lifetime for lanthanide participation is set by the lanthanide emission decay. The expected variation of the lifetime, τ_{obs}, in coordination polymers and MOFs is about 100 and 2000 μs for Eu^{III} and Tb^{III}; the lifetime of Eu^{III} is typically longer than that of Tb^{III}.[12c,19] In molecular complexes, for example, solvent molecules, such as H_2O, lead to a decrease in the observed lifetimes on the scale of 100–1500 μs, depending on the amount of coordinated molecules. For Ln@IFP-6, we assume a mixture of effects, leading to the biexponential decay in the range of 200–1400 μs, because there are various ways of coordinating incorporated Ln^{III} ions with solvent molecules and counterions, and interactions with the MOF backbone in the channels. The findings again corroborate the incorporation of Ln^{III} ions into Ln@IFP-1.

A depiction of the samples under UV light ($\lambda_{exc} = 365$ nm) shows a blue emission color for IFP-6 (Figure 8). Incorporation of the Ln ions results in different emission colors. For Tb@IFP-6 and Eu@IFP-6, the observable emission changes to greenish and reddish colors, respectively. The Sm^{III} emission, however, is too weak in Sm@IFP-6 to cause a color shift.

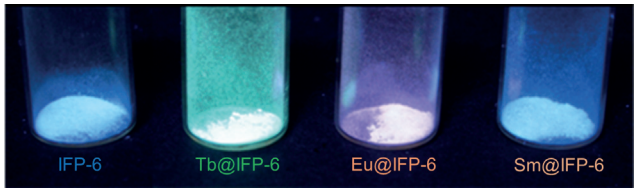

Figure 8. Photographs of as-synthesized IFP-6 and Ln@IFP-6 with UV-light excitation ($\lambda_{exc} = 365$ nm).

Conclusion

We have employed a rare example of an imidazolate anion based IL as a linker precursor for the fabrication of a MOF, IFP-6, in DMF. Such modification of a linker to an IL could be useful in the future for other tri- and tetrazoles or derivatives. IFP-6 showed low performance for N_2, H_2, and CH_4 uptake from vacuum to atmospheric pressure at various temperatures, although the channel diameter was higher than the molecular sizes of the gases and the bulk MOF exhibited structural integrity after solvent removal. At elevated pressure, CO_2 and CH_4 was taken up by the pores of IFP-6, and the respective uptake capacities were comparable to Zn^{II}-based isostructural IFP-1. For a deeper understanding of the porosity, we performed PALS investigations to demonstrate the unique ability of exposing nanoscale porosity; this vindicated the supposition that the presence of inner pores in IFP-6 were comparable to those of IFP-1. From the annealing behavior, the intensities inside the pores (I_4) for IFP-6 decreased, which could be attributed to filling of the pore apertures. In-depth porosimetry studies by using PALS have so far been performed for very few MOFs, such as MOF-5 and Zn-HKUST-1. From the results for IFP-6, it can be inferred that the channels to the inner pores are blocked by amorphous parts and defects in IFP-6 that are inherently formed upon removal of the water molecules coordinated to Cd^{II}. Hence, diffusion of gas molecules is only possible at elevated pressure, which forces gases through these barriers into the retained inner pores.

Furthermore, the in situ formation of IFP-6 can be successfully coupled with an in situ loading with trivalent ions (Ln^{III} = Tb, Eu, and Sm). The rare-earth ions are located within the channels of the MOFs without specific positions. Doping results in further luminescence properties because the lanthanide ions are included in the luminescence process. This is achieved by antenna effects of the MOF, including energy transfer from the framework linker to the lanthanide ions followed by subsequent emission from 4f levels of the rare-earth ions. The antenna effect is of different efficiency for $Tb^{III} > Eu^{III} > Sm^{III}$ for IFP-6 and has proven superior to that of isostructural Ln@IFP-1, despite the short lifetime of the MOF linker.

Experimental Section

Materials and synthesis

Ln^{III} nitrates ($Tb(NO_3)_3 \cdot 5H_2O$ 99.9% trace-metals basis, $Eu(NO_3)_3 \cdot 5H_2O$ 99.99% trace-metals basis, and $Sm(NO_3)_3 \cdot 6H_2O$) were purchased form Aldrich. DMF was purchased from VWR International. All reagents and solvents were used without further purification. The linker precursor, IL1,[21] and IFP-1[20a] were synthesized according to published procedures (see the Supporting Information for details). For details on the instrumentation and analytical investigations, see the Supporting Information.

Synthesis of IFP-6

In a sealed tube (type A, company: Ace), IL1 (0.075 g, 0.23 mmol) and $Cd(OAc)_2 \cdot 2H_2O$ (0.12 g, 0.46 mmol) were dissolved in DMF (6 mL). The tube was closed and the mixture was heated at 130 °C for 48 h (Scheme 1). After cooling the mixture to RT, fine colorless crystals of IFP-6 were obtained by filtration, washed with DMF three times, and dried in air (≈48% based on $Cd(OAc)_2 \cdot 2H_2O$). IR (KBr pellet): $\tilde{\nu} = 3319$ (m), 3072 (m), 1665 (s), 1564 (vs), 1439 (m), 1266 (m), 1220 (m), 1113 (m), 815 (m), 743 cm^{-1} (m); elemental analysis calcd (%) for $C_6H_6CdN_4O_2$: C 25.87, H 2.17, N 20.11; found: C 25.58, H 1.97, N 20.31.

Synthesis of Ln@IFP-6 (Ln^{III} = Tb, Eu, and Sm)

The reaction mixture, containing $Cd(OAc)_2 \cdot 2H_2O$ (0.122 g, 0.46 mmol), $Ln(NO_3)_3 \cdot xH_2O$ ($Tb(NO_3)_3 \cdot 5H_2O$ (0.100 g, 0.23 mmol), $Eu(NO_3)_3 \cdot 5H_2O$ (0.098 g, 0.23 mmol), or $Sm(NO_3)_3 \cdot 6H_2O$(0.102 g, 0.23 mmol)), and IL1 (0.075 g, 0.23 mmol) dissolved in DMF (7 mL), was sealed in a tube. The reaction mixtures were then treated as described above. Physical characterization of the materials was achieved by elemental analysis, ICP-OES, and powder XRD (see the Supporting Information for details).

Acknowledgements

We thank Dr. C. Günter (Universität Potsdam) for help with X-ray powder diffraction measurements and Prof. C. Jäger (BAM Federal Institute for Materials Research and Testing, Berlin, Germany) for solid-state NMR spectroscopy measurements. This work is financially supported by the German Research Foundation (SPP 1362 "Porous Metal-Organic Frameworks," HO 1706/7-1, HO 1706/7-2 and MU-1562/5-1 as well as MU-1562/5-2).

Keywords: adsorption · cadmium · ionic liquids · luminescence · metal–organic frameworks

[1] H.-C. Zhou, J.; Park, Z. Y. U. Wang, L. B. Sun, Y. P. Chen, H. C. Zhou, *J. Am. Chem. Soc.* **2012**, *134*, 20110 – 20116 R. Long, O. M. Yaghi, *Chem. Rev.* **2012**, *112*, 673 – 674.

[2] H.-C. Zhou, S. Kitagawa, *Chem. Soc. Rev.* **2014**, *43*, 5415 – 5418.

[3] a) K. S. Walton, R. Q. Snurr, *J. Am. Chem. Soc.* **2007**, *129*, 8552 – 8656; b) T. Düren, Y. S. Bae, R. Q. Snurr, *Chem. Soc. Rev.* **2009**, *38*, 1237 – 1247; c) J. K. Schnobrich, K. Koh, K. N. Sura, A. J. Matzger, *Langmuir* **2010**, *26*, 5808 – 5814; d) C. S. Lim, J. K. Schnobrich, A. G. Wong-Foy, A. J. Matzger, *Inorg. Chem.* **2010**, *49*, 5271 – 5275.

[4] a) J. Hafizovic, M. Bjørgen, U. Olsbye, P. D. C. Dietzel, S. Bordiga, C. Prestipino, C. Lamberti, K. P. Lillerud, *J. Am. Chem. Soc.* **2007**, *129*, 3612 – 3620; b) J. Zhao, D.-S. Li, X.-J. Ke, B. Liu, K. Zou, H.-M. Hu, *Dalton Trans.* **2012**, *41*, 2560 – 2563; c) J. I. Feldblyum, D. Dutta, A. G. Wong-Foy, A. Dailly, J. Imirzian, D. W. Gidley, A. J. Matzger, *Langmuir* **2013**, *29*, 8146 – 8153.

[5] K. Barthelet, J. Marrot, G. Férey, D. Riou, *Chem. Commun.* **2004**, 520 – 521.

[6] a) J. E. Mondloch, M. J. Katz, N. Planas, D. Semrouni, L. Gagliardi, J. T. Hupp, O. K. Farha, *Chem. Commun.* **2014**, *50*, 8944 – 8946; b) L. Q. Ma, A. Jin, Z. G. Xie, W. B. Lin, *Angew. Chem. Int. Ed.* **2009**, *48*, 9905 – 9908; *Angew. Chem.* **2009**, *121*, 10089 – 10092.

[7] A. P. Nelson, O. K. Farha, K. L. Mulfort, J. T. Hupp, *J. Am. Chem. Soc.* **2009**, *131*, 458 – 460.

[8] J. I. Feldblyum, M. Liu, D. W. Gidley, A. J. Matzger, *J. Am. Chem. Soc.* **2011**, *133*, 18257 – 18263.

[9] a) D. W. Gidley, H.-G. Peng, R. S. Vallery, *Annu. Rev. Mater. Res.* **2006**, *36*, 49 – 79; b) Y. Kobayashi, K. Ito, T. Oka, K. Hirata, *Radiat. Phys. Chem.* **2007**, *76*, 224 – 230.

[10] M. Liu, A. G. Wong-Foy, R. S. Vallery, W. E. Frieze, J. K. Schnobrich, D. W. Gidley, A. J. Matzger, *Adv. Mater.* **2010**, *22*, 1598 – 1601.

[11] a) M. D. Allendorf, C. A. Bauer, R. K. Bhakta, R. J. T. Houk, *Chem. Soc. Rev.* **2009**, *38*, 1330 – 1352; b) J. Rocha, L. D. Carlos, F. A. Almeida Paz, D. Ananias, *Chem. Soc. Rev.* **2011**, *40*, 926 – 940; c) Y. Cui, Y. Yue, G. Qian, B. Chen, *Chem. Rev.* **2012**, *112*, 1126 – 1162.

[12] a) K. Müller-Buschbaum, *Group 3 Elements and Lanthanide Metals in The Chemistry of Metal-Organic Frameworks - Synthesis Characterization, and Applications* (Ed.: S. Kaskel), Wiley-VCH, Weinheim, **2016**; b) K. Müller-Buschbaum, F. Beuerle, C. Feldmann, *Microporous Mesoporous Mater.* **2015**, *216*, 171 – 199; c) J. Heine, K. Müller-Buschbaum, *Chem. Soc. Rev.* **2013**, *42*, 9232 – 9242.

[13] a) D. Liu, K. Lu, C. Poon, W. Lin, *Inorg. Chem.* **2014**, *53*, 1916 – 1924; b) Q.-Y. Yang, M. Pan, S.-C. Wei, Kang Li, B.-B. Du, C.-Y. Su, *Inorg. Chem.* **2015**, *54*, 5707 – 5716; c) Y.-H. Zhang, X. Li, S. Song, *Chem. Commun.* **2013**, *49*, 10397 – 10399; d) Z.-F. Liu, M.-F. Wu, S.-H. Wang, F.-K. Zheng, G.-E. Wang, J. Chen, Y. Xiao, A.-Q. Wu, G.-C. Guo, J.-S. Huang, *J. Mater. Chem. C* **2013**, *1*, 4634 – 4639; e) Y. Zhou, B. Yan, F. Lei, *Chem. Commun.* **2014**, *50*, 15235 – 15238; f) C. Feng, J.-W. Sun, P.-F. Yan, Y.-X. Li, T.-Q. Liu, Q.-Y. Sun, G.-M. Li, *Dalton Trans.* **2015**, *44*, 4640 – 4647; g) J. Chen, Q. Zhang, Z.-F. Liu, S.-H. Wang, Y. Xiao, R. Li, J.-G. Xu, Y.-P. Zhao, F.-K. Zheng, G.-C. Guo, *Dalton Trans.* **2015**, *44*, 10089 – 10096.

[14] a) R.-Y. Chen, D. Tian, Y.-W. Li, Y.-B. Lv, H.-W. Sun, Z. Chang, X.-H. Bu, *RSC Adv.* **2015**, *5*, 24655 – 24660; b) F. Luo, S. R. Batten, *Dalton Trans.* **2010**, *39*, 4485 – 4488; c) Q. Tang, S. Liu, Y. Liu, D. He, J. Miao, X. Wang, Y. Ji, Z. Zheng, *Inorg. Chem.* **2014**, *53*, 289 – 293; d) D. F. Sava, L. E. S. Rohwer, M. A. Rodriguez, T. M. Nenoff, *J. Am. Chem. Soc.* **2012**, *134*, 3983 – 3986.

[15] a) Y. Xiao, S.-H. Wang, F.-K. Zheng, M.-F. Wu, J. Xu, Z.-F. Liu, J. Chen, R. Li, G.-C. Guo, *CrystEngComm* DOI: 10.1039/c5ce02140e; b) S.-N. Zhao, L.-J. Li, X.-Z. Song, M. Zhu, Z.-M. Hao, X. Meng, L.-L. Wu, J. Feng, S.-Y. Song, C. Wang, H.-J. Zhang, *Adv. Funct. Mater.* **2015**, *25*, 1463 – 1469; c) T.-W. Duan, B. Yan, *J. Mater. Chem. C* **2015**, *3*, 2823 – 2830; d) A. Zurawski, M. Mai, D. Baumann, C. Feldmann, K. Müller-Buschbaum, *Chem. Commun.* **2011**, *47*, 496 – 498; e) J.-C. Rybak, M. Hailmann, P. R. Matthes, A. Zurawski, J. Nitsch, A. Steffen, J. G. Heck, C. Feldmann, S. Götzendörfer, J. Meinhardt, G. Sextl, H. Kohlmann, S. J. Sedlmaier, W. Schnick, K. Müller-Buschbaum, *J. Am. Chem. Soc.* **2013**, *135*, 6896 – 6902.

[16] a) A. Ablet, S.-M. Li, W. Cao, X.-J. Zheng, W.-T. Wong, L.-P. Jin, *Chem. Asian J.* **2013**, *8*, 95 – 100; b) Y. Liu, M. Pan, Q.-Y. Yang, L. Fu, K. Li, S.-C. Wei, C.-Y. Su, *Chem. Mater.* **2012**, *24*, 1954 – 1960; c) C.-Y. Sun, X.-L. Wang, X. Zhang, C. Qin, P. Li, Z.-M. Su, D.-X. Zhu, G.-G. Shan, K.-Z. Shao, H. Wu, J. Li, *Nat. Commun.* DOI:10.1038/ncomms3717; d) J.-S. Qin, S.-R. Zhang, D.-Y. Du, P. Shen, S.-J. Bao, Y.-Q. Lan, Z.-M. Su, *Chem. Eur. J.* **2014**, *20*, 5625 – 5630; e) S. Bhattacharyya, A. Chakraborty, K. Jayaramulu, A. Hazra, T. K. Maji, *Chem. Commun.* **2014**, *50*, 13567 – 13570; f) S. Roy, A. Chakraborty, T. K. Maji, *Coord. Chem. Rev.* **2014**, *273*, 139 – 164.

[17] a) Y.-Y. Jiang, S.-K. Ren, J.-P. Ma, Q.-K. Liu, Y.-B. Dong, *Chem. Eur. J.* **2009**, *15*, 10742 – 10746; b) C.-X. Chen, Q.-K. Liu, J.-P. Ma, Y.-B. Dong, *J. Mater. Chem.* **2012**, *22*, 9027 – 9033; c) J. An, C. M. Shade, D. A. Chengelis-Czegan, S. Petoud, N. L. Rosi, *J. Am. Chem. Soc.* **2011**, *133*, 1220 – 1223.

[18] J.-S. Qin, S.-J. Bao, P. Li, W. Xie, D. Y. Du, Z. Liang, Y.-Q. Lan, Z.-M. Su, *Chem. Asian J.* **2014**, *9*, 749 – 753.

[19] S. S. Mondal, K. Behrens, P. R. Matthes, F. Schönfeld, J. Nitsch, A. Steffen, P.-A. Primus, M. U. Kumke, K. Müller-Buschbaum, H.-J. Holdt, *J. Mater. Chem. C* **2015**, *3*, 4623 – 4631.

[20] a) F. Debatin, A. Thomas, A. Kelling, N. Hedin, Z. Bacsik, I. Senkovska, S. Kaskel, M. Junginger, H. Müller, U. Schilde, C. Jäger, A. Friedrich, H.-J. Holdt, *Angew. Chem. Int. Ed.* **2010**, *49*, 1258 – 1262; *Angew. Chem.* **2010**, *122*, 1280 – 1284; b) S. S. Mondal, A. Thomas, H.-J. Holdt, *Microporous Mesoporous Mater.* **2015**, *216*, 2 – 12; c) K. Behrens, S. S. Mondal, R. Nöske, I. A. Baburin, S. Leoni, C. Günter, J. Weber, H.-J. Holdt, *Inorg. Chem.* **2015**, *54*, 10073 – 10080; d) S. S. Mondal, A. Bhunia, I. A. Baburin, C. Jäger, A. Kelling, U. Schilde, G. Seifert, C. Janiak, H.-J. Holdt, *Chem. Commun.* **2013**, *49*, 7599 – 7601; e) S. S. Mondal, A. Bhunia, A. Kelling, U. Schilde, C. Janiak, H.-J. Holdt, *Chem. Commun.* **2014**, *50*, 5441 – 5443; f) S. S. Mondal, S. Dey, I. A. Baburin, A. Kelling, U. Schilde, G. Seifert, C. Janiak, H.-J. Holdt, *CrystEngComm* **2013**, *15*, 9394 – 9399.

[21] S. S. Mondal, H. Müller, M. Junginger, A. Kelling, U. Schilde, V. Strehmel, H.-J. Holdt, *Chem. Eur. J.* **2014**, *20*, 8170 – 8181.

[22] a) R. E. Morris, *Chem. Commun.* **2009**, 2990 – 2998; b) E. R. Parnham, R. E. Morris, *Acc. Chem. Res.* **2007**, *40*, 1005 – 1013; c) R. E. Morris, X. Bu, *Nat. Chem.* **2010**, *2*, 353 – 361; d) Z. Lin, D. S. Wragg, J. E. Warren, R. E. Morris, *J. Am. Chem. Soc.* **2007**, *129*, 10334 – 10335.

[23] a) Z. Lin, D. S. Wragg, R. E. Morris, *Chem. Commun.* **2006**, 2021 – 2023; b) D. N. Dybtsev, H. Chun, K. Kim, *Chem. Commun.* **2004**, 1594 – 1595; c) E. R. Parnham, R. E. Morris, *J. Mater. Chem.* **2006**, *16*, 3682 – 3684.

[24] S. S. Mondal, A. Bhunia, S. Demeshko, A. Kelling, U. Schilde, C. Janiak, H.-J. Holdt, *CrystEngComm* **2014**, *16*, 39 – 42.

[25] a) C.-H. Lee, H.-Y. Huang, Y.-H. Liu, T.-T. Luo, G.-H. Lee, S.-M. Peng, J.-C. Jiang, I. Chao, K.-L. Lu, *Inorg. Chem.* **2013**, *52*, 3962 – 3968; b) C.-H. Lee, J.-Y. Wu, G.-H. Lee, S.-M. Peng, J.-C. Jiang, K.-L. Lu, *Inorg. Chem. Front.* **2015**, *2*, 477 – 484; c) F. Luo, M.-S. Wang, M.-B. Luo, G.-M. Sun, Y.-M. Song, P.-X. Lia, G.-C. Guo, *Chem. Commun.* **2012**, *48*, 5989 – 5991; d) B. Zheng, J. Bai, J. Duan, L. Wojtas, M. J. Zaworotko, *J. Am. Chem. Soc.* **2011**, *133*, 748 – 751.

[26] a) Y. Xiong, Y.-Z. Fan, R. Yang, S. Chen, M. Pan, J.-J. Jiang, C.-Y. Su, *Chem. Commun.* **2014**, *50*, 14631 – 14634; b) J. An, R. P. Fiorella, S. J. Geib, N. L. Rosi, *J. Am. Chem. Soc.* **2009**, *131*, 8401 – 8403; c) B. Liu, D.-S. Li, L. Hou, G.-P. Yang, Y.-Y. Wang, Q.-Z. Shi, *Dalton Trans.* **2013**, *42*, 9822 – 9825; d) B. Liu, R. Zhao, K. Yue, J. Shi, Y. Yu, Y. Wang, *Dalton Trans.* **2013**, *42*, 13990 – 13996; e) R. Haldar, S. K. Reddy, V. M. Suresh, S. Mohapatra, S. Balasubramanian, T. K. Maji, *Chem. Eur. J.* **2014**, *20*, 4347 – 4356.

[27] F. Debatin, J. Möllmer, S. S. Mondal, K. Behrens, A. Möller, R. Staudt, A. Thomas, H.-J. Holdt, *J. Mater. Chem.* **2012**, *22*, 10221 – 10227.

[28] Y. Zou, S. Hong, M. Park, H. Chun, M. S. Lah, *Chem. Commun.* **2007**, 5182 – 5184.

[29] a) Z. Fang, B. Bueken, D. E. De Vos, R. A. Fischer, *Angew. Chem. Int. Ed.* **2015**, *54*, 7234 – 7254; *Angew. Chem.* **2015**, *127*, 7340 – 7362; b) J. Canivet, M. Vandichel, D. Farrusseng, *Dalton Trans.* **2016**, *45*, 4090 – 4099; c) A. K. Cheetham, T. D. Bennett, F.-X. Coudert, A. L. Goodwin, *Dalton Trans.* **2016**, *45*, 4113 – 4126; d) A. W. Thornton, R. Babarao, A. Jain, F. Trousselet, F.-X. Coudert, *Dalton Trans.* **2016**, *45*, 4352 – 4359.

[30] a) O. V. Gutov, M. G. Hevia, E. C. Escudero-Adán, A. Shafir, *Inorg. Chem.* **2015**, *54*, 8396 – 8400; b) J.; Park, Z. Y. U. Wang, L. B. Sun, Y. P. Chen, H. C. Zhou, *J. Am. Chem. Soc.* **2012**, *134*, 20110 – 20116; c) E. López-Maya, C. Montoro, V. Colombo, E. Barea, J. A. R. Navarro, *Adv. Funct. Mater.* **2014**, *24*, 6130 – 6135; d) C. A. Trickett, K. J. Gagnon, S. Lee, F. Gándara, H.-B. Bürgi, O. M. Yaghi, *Angew. Chem. Int. Ed.* **2015**, *54*, 11162 – 11167; *Angew. Chem.* **2015**, *127*, 11314 – 11319; e) U. Ravon, M. Savonnet, S. Aguado, M. E. Domine, E. Janneau, D. Farrusseng, *Microporous Mesoporous Mater.* **2010**, *129*, 319 – 329; f) H. Furukawa, U. Müller, O. M. Yaghi, *Angew. Chem. Int. Ed.* **2015**, *54*, 3417 – 3430; U. Müller, O. M. Yaghi, *Angew. Chem. Int. Ed.* **2015**, *54*, 3417 – 3430; *Angew. Chem.* **2015**, *127*, 3480 – 3494; g) E. López-Maya, C. Montoro, L. M. Rodríguez-Albelo, S. D. A. Cervantes, A. A. Lozano-Pérez, J. L. Cenís, E. Barea, J. A. R. Navarro, *Angew. Chem. Int. Ed.* **2015**, *54*, 6790 – 6794; *Angew. Chem.* **2015**, *127*, 6894 – 6898; h) W. Liang, C. J. Coghlan, F. Ragon, M. Rubio-Martinez, D. M. D'Alessandro, R. Babarao, *Dalton Trans.* **2016**, *45*, 4496-4500.

[31] S.-R. Zheng, S.-L. Cai, Q.-Y. Yang, T.-T. Xia, J. Fan, W.-G. Zhang, *Inorg. Chem. Commun.* **2011**, *14*, 826 – 830.

Received: November 25, 2015
Published online on April 1, 2016